한국동력기계공학회지 제10권 제1호 pp.25~33 2006년 2월

45° 경사진 거칠기가 설치된 채널에서 유체유동과 열전달에 대한 수치모사

Numerical Simulation for Heat Transfer and Fluid Flow in the Channel with 45° Incinlined Rib

오세경 · 강호근 · 안수환 · 김명호 · 배성택

S. K. Oh, H. K. Kang, S. W. Ahn, M. H. Kim and S. T. Bae

Key Words : Numerical Simulation(수치모사), Rough Walls(거친 벽), Square Duct(사각덕트), 45° Inclined Rib(45° (경사진 거칠기), Heat Transfer(열전달), Pressure Drop(압력강하)

요 약 : 거칠기가 한 벽면과 두 벽면에 설치된 사각채널에서 비압축성 유체유동과 열전달을 조사하기위해 3차원 수치모사를 행하였다. CFX (version 5) software package 를 사용하여 계산하였다. 거친 벽은 45°경사진 거칠기가 설치되어 있다. 채널의 4 벽면은 일정한 열 유속으로 가열하였다. 수치계산 결과는 실험값과 잘 일치 하였다. 연구의 조건은 거칠기 피치와 높이의 비가 8이고, 거칠기 높이와 채널 수력직경의 비가 0.067이며, 레이놀즈수의 범위는 7,600에서 24,900이었다. 연구의 결과는 열전달계수와 마찰계수는 사각채널에서 거친 벽면의 수가 클수록 증가 함을 보였다.

1. Introduction

Many studies therefore have been carried out for the heat transfer in ribbed channels and various types of ribs have been tested. A standard case of full-span ribs attached perpendicularly to the flow direction has been the first target and its friction and heat transfer characteristics have been reported[1,2]. Further studies were made for other cases of attaching oblique ribs and V-shaped ribs to the channel wall. In these cases, secondary flow is incurred in the channel and enhances the fluid mixing between the near wall and core regions in the channel, eventually resulting in the enhancement of local heat transfer at the channel walls[3-5]

Accurate evaluation of heat loads in the components of a gas-turbine engine is a key factor in the development of new and efficient engines. Common design techniques utilize experimental correlations to quickly estimate the heat transfer coefficients[6]. These methods do not reveal the underlying mechanism of turbulence and heat transfer for the device in question. They often are inaccurate. Owing to advances in available computer resources, an elaborate numerical techniques, based on the solution of the full 3D Reynolds averaged Navier-Stokes (RANS) equations, are now being used to shed light on the flow phenomena and to provide guidelines to improve design methodology. In the RANS approach, the Navier-Stokes equations are averaged and the Reynolds Stresses are computed with a turbulence model. The present model is chosen the $k-\varepsilon$ two equation turbulence model.

In the present article, some results of the three-dimensional numerical computation using a commercial software package of CFX code (version 5.0) and the experiment conducted for flow and thermal fields over two types of array of ribs attached to a channel wall are presented; one is of one-sided ribs and the other is of two-opposite-sided ribs, where both arrays are

접수일 : 2005년 12월 2일

안수환(책임저자) : 경상대학교 기계항공공학부 해양산업연구소
E-mail : swahn@gssnu.ac.kr Tel. 055-640-3125
오세경, 강호근, 김명호: 경상대학교 기계항공공학부
배성택 : 주식회사 태건

attached in a position 45° inclined to the flow direction. The discussion are given to the effects of three-dimensionality and unsteadiness of the thermal fields for twofold purposes, one to test the applicability of numerical study to the type of flow under concern and another to provide the experimental data to prove the numerical prediction.

2. Mathematical Formulation

The governing equations used in the present numerical study are the three-dimensional, time dependent continuity, momentum and energy equations employing a turbulence model for unsteady Navier-Stokes equation in CFX code (version 5). The current research utilizes the $k-\varepsilon$ two equation turbulence model by Jones and Launder[7,8] for the Reynolds stress based upon the eddy viscosity introduced in the Boussinesq approximation[9].

In general, turbulence models seek to modify the original unsteady Navier-Stokes equations by the introduction of averaged and fluctuating quantities to produce the Reynolds Averaged Navier-Stokes (RANS) equations. These equations represent the mean flow quantities only, while modeling turbulence effects without a need for the resolution of the turbulent fluctuations. A velocity U may be divided into an average component, $\overline{U}$, and a time varying component, u.

$$U = \overline{U} + u \tag{1}$$

The averaged component is given by,

$$\overline{\mathbf{U}} = \frac{1}{\Delta t}\int_{t}^{t+\Delta t} \mathbf{U}\, dt \tag{2}$$

where Δt is a time scale that is large relative to the turbulent fluctuations, but small relative to the time scale to which the equations are solved.

Two-equation turbulence model is very widely used, as it offers a good compromise between numerical effort and computational accuracy. Both the velocity and length scale are solved using separate transport equations. Then the continuity and momentum equations are as follows.

$$\frac{\partial \rho}{\partial t} + \nabla \cdot (\rho \mathbf{U}) = 0 \tag{3}$$

$$\frac{\partial \rho \mathbf{U}}{\partial t} + \nabla \cdot (\rho \mathbf{U} \otimes \mathbf{U}) - \nabla \cdot (\mu_{eff} \nabla \mathbf{U}) = \nabla p' + \nabla \cdot (\mu_{eff} \nabla U)^T + B \tag{4}$$

Here, B is the sum of body forces, μ_{eff} is the effective viscosity accounting for turbulence, and p' is the modified pressure given by

$$p' = p + \frac{2}{3}\rho k \tag{5}$$

The $k-\varepsilon$ model is based on the eddy viscosity concept, so that

$$\mu_{eff} = \mu + \mu_t \tag{6}$$

where μ_t is the eddy viscosity. The $k-\varepsilon$ model assumes that the turbulence viscosity is linked to the turbulence kinetic energy and dissipation via the relation. Therefore in the standard $k-\varepsilon$ model the eddy viscosity is specified by

$$\mu_t = \frac{\rho C_\mu k^2}{\varepsilon} \tag{7}$$

and the system is closed, provided equations are known for k and ε. The model proposed by Jones and Launder[7,8] provides approximate equations for k and ε such that the system is closed. The values of k and ε come directly from the differential transport equations for turbulence kinetic energy and turbulence dissipation rate as follows.

$$\frac{\partial (\rho k)}{\partial t} + \nabla \cdot (\rho \mathbf{U} k) = \nabla \cdot \left[\left(\mu + \frac{\mu_t}{\sigma_k}\right)\nabla k\right] + P_k - \rho\varepsilon \tag{8}$$

$$\frac{\partial (\rho \varepsilon)}{\partial t} + \nabla \cdot (\rho \mathbf{U} \varepsilon) = \nabla \cdot \left[\left(\mu + \frac{\mu_t}{\sigma_\varepsilon}\right)\nabla \varepsilon\right] + \frac{\varepsilon}{k}(C_{\varepsilon 1} P_k - C_{\varepsilon 2}\rho\varepsilon) \tag{9}$$

Here, to assure results for flows in which no wall interaction is encountered, the standard $k-\varepsilon$ model closure coefficients are utilized[10]. And the closure coefficients for the $k-\varepsilon$ are also found by correlating with the experimental results of different flow fields, including the far wake, mixing layer and jet[11]:

$$C_\mu = 0.09\ ,\ C_{\varepsilon 1} = 1.44\ ,\ C_{\varepsilon 2} = 1.92\ ,$$
$$\sigma_k = 1.0 \text{ and } \sigma_\varepsilon = 1.3 \tag{10}$$

And P_k is the turbulence production due to viscous and buoyancy forces, which is modeled by

$$P_k = \mu_t \nabla \mathbf{U} \cdot \left(\nabla \mathbf{U} + \nabla \mathbf{U}^T\right) \tag{11}$$

The Reynolds-averaged energy equation is expressed by

$$\frac{\partial \rho i_{tot}}{\partial t} + \nabla \cdot \left(\rho U i_{tot} + \rho \overline{\mathbf{u} i} - \lambda \nabla T\right) = \frac{\partial p}{\partial t} \tag{12}$$

in which λ is thermal conductivity and i_{tot} is defined as the mean total enthalpy, which is given in terms of the specific static enthalpy, i, by,

$$i_{tot} = i + \frac{1}{2}U^2 + k \tag{13}$$

In addition to the mean flow kinetic energy, the total enthalpy contains a contribution from the turbulent kinetic energy, k, given by

$$k = \frac{1}{2}\overline{\left(u'^2 + v'^2 + w'^2\right)} \tag{14}$$

3. Experimental Apparatus and Numerical Conditions

3.1 Experimental Apparatus and Procedure

Fig. 1 shows a schematic diagram of the test apparatus. A 195W blower delivered laboratory air through an 81.6mm diameter flexible tube at room temperature. The air then passed through an orifice to measure flow rates, through a long straight square channel with a hydraulic diameter of D_h = 30 mm and length of L_h= 900 mm, and finally through the heated square test channel with D_h = 30 mm and length L = 1800 mm. The entrance section was long enough to ensure a hydrodynamically fully developed flow just before the heated test channel. The air was exhausted into the atmosphere at the end of the test channel.

The test channel is shown in Fig. 2. It was constructed of four 5-mm-thick aluminum plates, and it had a cross-section of 30x30 mm. The aluminum plates were separated by 0.8-mm-thick fiber to reduce the conduction heat loss and to obtain an average heat transfer coefficient. Square sharp-edged aluminum ribs with a height of e = 2 mm (e/D_h = 0.067) and an equal spacing of p = 16 mm (p/e = 8) were glued with silicone adhesive onto the channel walls. As shown in Fig. 3, the ribs were positioned with an inclination angle of 45°. The entire test section was covered tightly with 50-mm-thick wood insulation. The channel walls were heated individually with electric woven heaters that were embedded and placed flat between the aluminum and wood plates to ensure good thermal contact. A transformer controlled the heaters independently so that a constant heat flux thermal boundary condition was created on
the channel walls.

Thermocouples embedded on the walls were used to measure the rib spanwise surface temperature at one downstream location in the test section to examine the temperature uniformity along the rib surface. The thermocouple beads were carefully embedded into the wall and then ground flat to ensure that they were flush with the surface. Wall temperatures along the axial direction of the four channel walls were measured using 40 copper constantan thermocouples. Five pressure taps were installed along the axial centerline of the walls to determine the pressure drop.

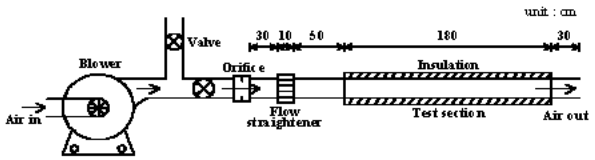

Fig. 1 Schematic diagram of test apparatus

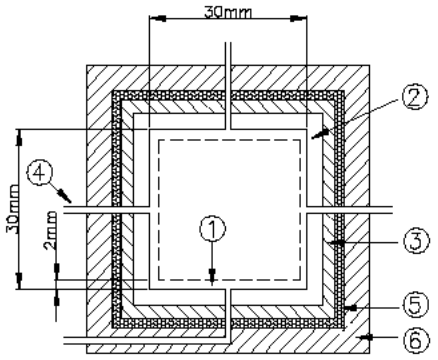

① Rib type roughness (height: 2mm) ④ Pressure tap
② Al plate (thickness: 5mm) ⑤ Gasket
③ Woven heater (Omega, USA) ⑥ Pine wood

Fig. 2 Details of the test section

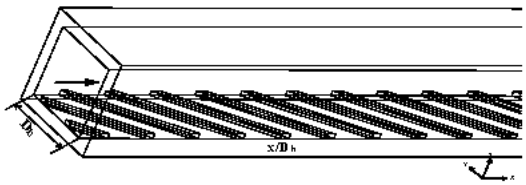

(a) One rib arrangement (case A)

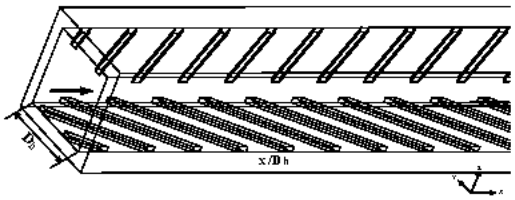

(b) Two ribs arrangement (case B)

Fig. 3 Rib arrangements on the wall

The friction factor for a fully developed flow in a square channel can be defined in terms of the dimensionless channel length (normalized by the hydraulic diameter, D_h), pressure drop, and air velocity as follows:

$$f_c = \Delta p / [4(L / D_h)(\rho u_b^2 / 2)] \quad (15)$$

The average ribbed channel friction factor, f_{ra}, is the weighted average of the four-sided smooth channel friction factor, f_{sm}, and the four-sided ribbed channel friction factor, f_{rs}. If the total wall area of the channel is C, the smooth wall area of the channel is C_{sm}, and the ribbed wall area of the channel is C_{rs}, then the average friction factor for a ribbed channel can be expressed as follows:

$$f_{ra} = f_{sm}(C_{sm} / C) + f_{rs}(C_{rs} / C) \quad (16)$$

The average ribbed channel friction factor was normalized by the friction factor for a fully developed turbulent flow in a smooth circular channel (with the channel diameter replaced by the hydraulic diameter of the square channel), as proposed by Blasius in[12] for Re < 50,000:

$$f_{ra} / f_{ss} = f_{ra} / (0.079 \ \mathrm{Re}^{-0.25}) \quad (17)$$

The heat transfer coefficient was calculated from the net heat transfer rate per unit surface area exposed to the cooling air($\dot{q}$), the wall temperature (T_w), and the bulk mean air temperature (T_b),

$$h = \dot{Q} / [A(T_w - T_b)] \quad (18)$$

where A is the total heat transfer area of the smooth walls (*i.e.*, excluding the surface area of the ribs). The heat transfer rate ($\dot{q}$) was defined as

$$\dot{Q} = \dot{m} C_p (T_{b2} - T_{b1}) \quad (19)$$

The Nusselt number was defined using the area-averaged heat transfer coefficient and the hydraulic diameter D_h for the square channel,

$$Nu = hD_h / \lambda \quad (20)$$

The Nusselt number for fully developed turbulent flow in a smooth channel has been correlated by Sieder and Tate[13].

$$Nu_{ss} = 0.027 \ \mathrm{Re}^{0.8} \mathrm{Pr}^{1/3} (\mu / \mu_w)^{0.14} \quad (21)$$

3.2 Numerical Conditions

Two configurations are considered in this

research. The dimension of square channel with one or two ribbed walls is shown in Fig. 2 (a) and (b), and all the length scales are normalized by the width of channel D_h(= 30 mm). For the hydrodynamic and heat transfer calculation, the computational domains are set for $0 \le x/D_h \le 25.0$, $0 \le y/D_h \le 1.0$, $0 \le z/D_h \le 1.0$, respectively. Grids used consist of about 490,000 (case A) and 550,000 (case B) hexahedral elements.

At an initial condition, air flows with , U_o = 4 m/s~13 m/s, corresponding to Re =7,600~25,00 based on D_h at the ambient temperature of $25\,^{0}C$. No-slip boundary conditions are employed on the walls and ribs, and an outflow condition is imposed on the outer far field boundary. Computations start with a uniform velocity $u_i(Ut/D_h = 0) = (U_0, 0, 0)$ at the channel inlet.

4. Results and Discussion

The heat transfer coefficients for a smooth channel were determined before performing tests in channels with ribbed walls for a benchmarking purpose. Fig. 4 shows the fully developed Nusselt numbers in a smooth channel at various Reynolds numbers. The empirical correlation by Sieder and Tate[13] is also plotted for a comparison. It is evident from Fig. 4 that there is excellent agreement between the existing correlation and our results.

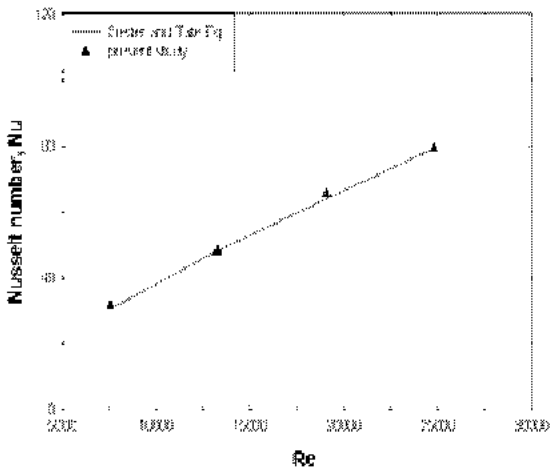

Fig. 4 Comparison of the Nusselt numbers in a smooth channel

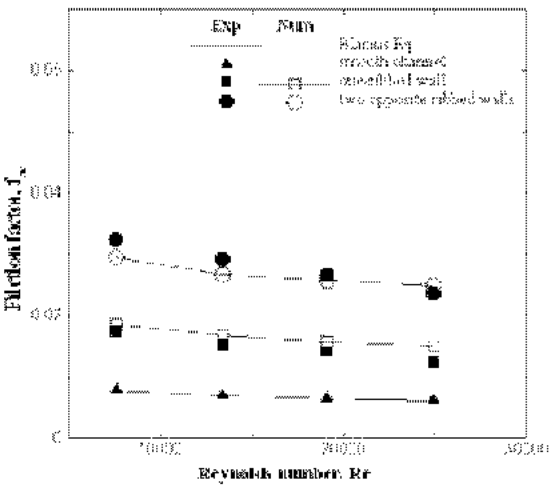

Fig. 5 Friction factor variation for different ribbed wall conditions

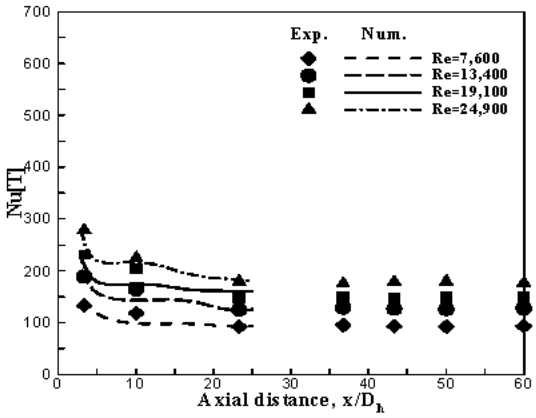

(a) Top side

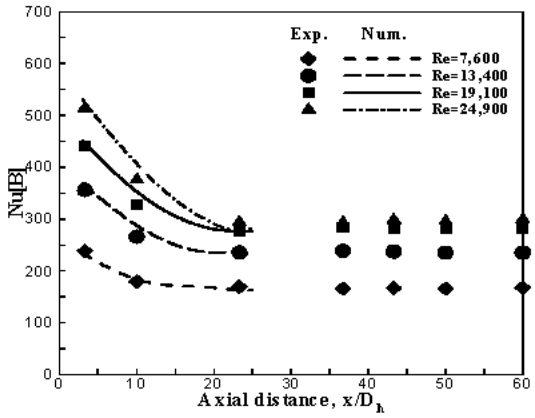

(b) Bottom side

Fig. 6 Local Nusselt number distributions in a channel with a ribbed bottom wall

Fig. 5 shows the channel averaged friction factors by obtaining from numerical and experimental data for one and two of ribbed walls at four Reynolds numbers ranging from 7,600 to

24,900. The empirical equation by Blasius for a smooth circular tube[12] is also included for comparison. The present results for a smooth channel agreed well with the Blasius correlation to within 2.5%. The results also showed that the friction factor decreased with increasing Reynolds number since the relative increase in the magnitude of the fluid velocity squared was greater than the increase in the wall shear stress with increasing Reynolds number. The friction factor increased with the number of ribbed walls. In particular, when two walls contained ribs, the maximum friction factor was nearly 3.6 times greater than the friction factor in the smooth channel, f_s at Re = 24,900. This was due to the greater flow resistance experienced with each additional ribbed wall, leading to higher friction values.

Figs. 6 and 9 show the Nusselt number distributions in square channels with ribbed walls as a function of the dimensionless axial location, x/D_h, for one and two walls with 45° inclined ribs oriented as shown in Fig. 3. The exact rib locations on the channel walls are shown in the square boxes. The letters B and T represent the bottom and top walls, respectively.

Fig. 6 compares the computed streamwise Nusselt number distributions with the experimental results for the test section with ribs only on the bottom wall. Computed results are observed to agree fairly well the experimental data.

In general, the Nusselt numbers decreased monotonically from its maximum value at the beginning of test section with increasing axial distance, eventually reaching a constant value at $L/D_h \cong 36$ where the flow was fully developed for the given Reynolds number. The results also showed that for all cases the local Nusselt numbers on both the ribbed and smooth walls increased with the Reynolds number. Hu and Shen[14] reported similar results in their study of square channel walls with 45° inclined discrete ribs.

Fig. 6 indicates that the Nusselt numbers on the ribbed bottom walls, Nu_s [B], were 1.8 to 3.8 times greater than the fully developed Nusselt numbers on a smooth wall correlated by Sieder and Tate[13] for Reynolds numbers ranging from 7,600 to 24,900. However, the Nusselt numbers on the ribbed side [B] were 58% greater than those on the opposite smooth side [T], respectively. The higher Nusselt numbers on the ribbed wall [B] were due to the increased level of turbulence generated by the ribs, which broke up the growth of the thermal boundary layer.

Fig. 7 shows the computed isothermal distributions in the channel with 45° inclined ribs only on the bottom wall at x/D_h =10 and 23. The contours of isothermal distributions at x/D_h=10 are more strongly concentrated to the position lower than those at x/D_h =23. It is supposed that the homogeneous flow at entrance is produced a turbulent flow at a restricted region by the secondary flow formed in the neighbourhood of the ribs at x/D_h =10, however, the turbulent flow is diffused to the whole region inside the channel at x/D_h =23.

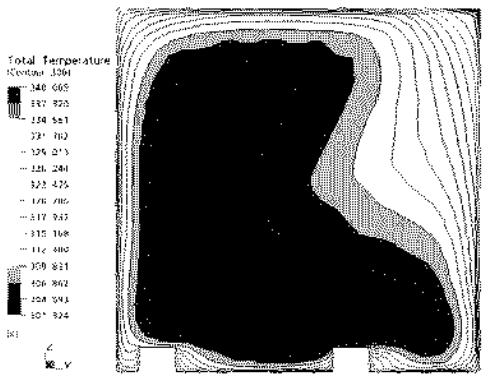

(a) x/D_h = 10 (300mm)

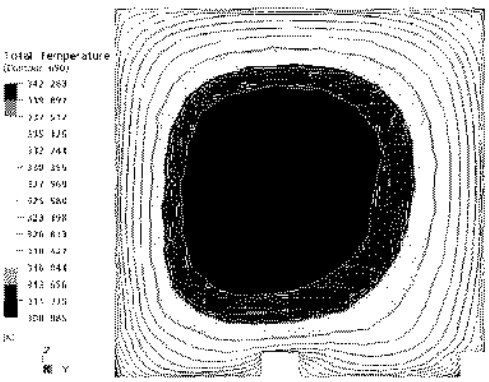

(b) x/D_h = 23 (690 mm)

Fig. 7 Temperature contours at y-z cross section of one-ribbed wall channel

Fig. 8 shows the streamwise Nusselt number distributions in the channel with ribs on two opposite sides the wall. The Nusselt numbers on the ribbed walls [T/B] were greater than those on the smooth walls [L/R], consistent with the behavior observed in Fig. 6.

The local Nusselt numbers in the channel with ribs on two opposite walls indicate the larger heat transfer enhancement.

This additional heat transfer enhancement is due to the larger increase in turbulence intensity resulting from more active mixing of the flow caused by the additional ribs.

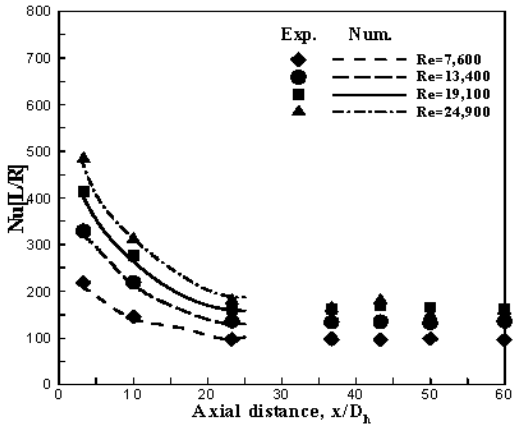

(a) Left and right side

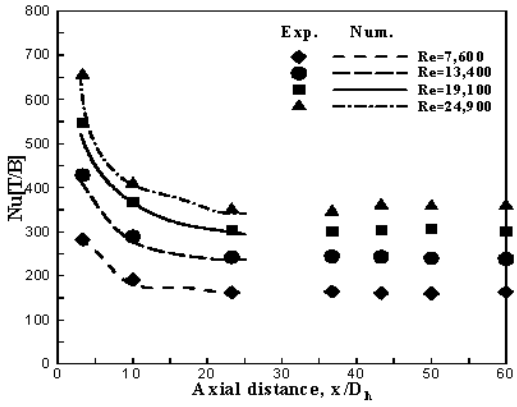

(b) Top and bottom side

Fig. 8 Local Nusselt number distributions in a channel with two opposite ribbed walls

Fig. 9 represents the contours of computed isothermal distributions in the channel with ribs on two opposite walls at x/D_h =10 and 23. On the contrary to Fig. 7, the isothermal distributions is almost unchanged along the axial distance between x/D_h =10 and 23. It is supposed that a turbulent flow is formed from the second flow generated by two opposite ribbed walls.

Figs. 10 and 11 show the contours of computed pressure distributions in the channels with ribs on one and two walls at x/D_h = 23. Fig. 11 shows the diagonally concentrated isobaric distributions, though Fig. 10 represents that the isobaric distributions are concentrated to the left hand side.

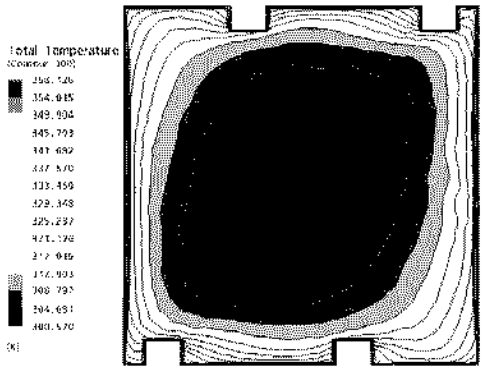

(a) x/D_h = 10 (300 mm)

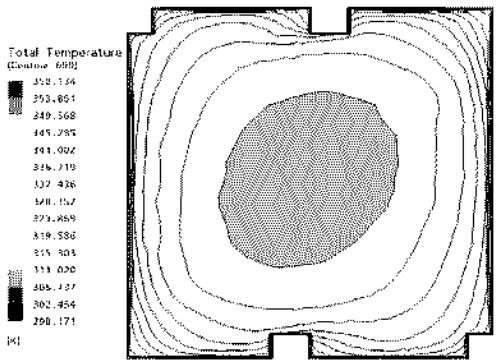

(b) $x/D_h = 23$ (690mm)

Fig. 9 Temperature contours at y-z cross section of two-opposite wall channel

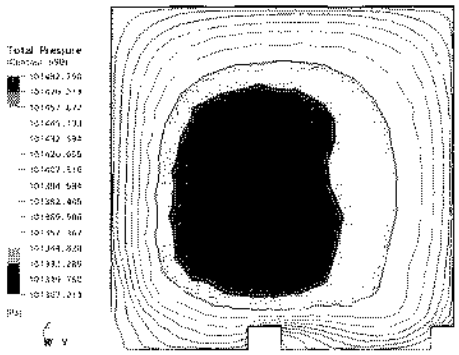

$x/D_h = 23$ (690mm)

Fig. 10 Pressure contours at y-z cross section of one-ribbed wall channel

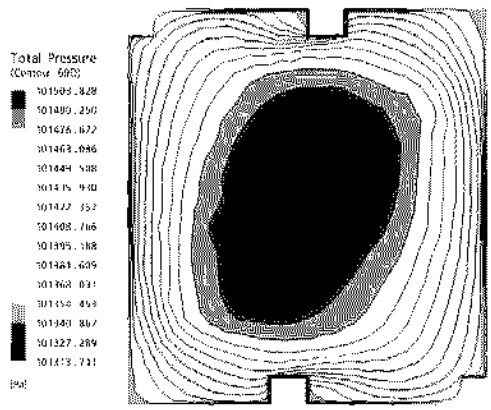

$x/D_h = 23$(690mm)

Fig. 11 Pressure contours at y-z cross section of two-ribbed wall channel

These trends may be attributed to the fact that the ribbed walls of the channel have the inclined ribs of attack angle of 45° as shown in Fig. 3.

6. Conclusion

The effects of the number of ribbed walls on the distribution of the heat transfer coefficients and friction factors in a square channel were numerically and experimentally investigated for Reynolds numbers ranging from 7,600 to 24,900. The following conclusions were drawn.

(1) In the channel with one ribbed wall, the Nusselt numbers on the ribbed side [B] were 58% greater than those on the opposite smooth side. The higher Nusselt numbers on the ribbed side [B] were due to the increased level of turbulence intensity generated by the ribs.

(2) The average friction factor increased with the number of ribbed walls. The friction factors obtained with ribs on two-opposite walls was nearly 3.6 times greater than those measured in a smooth channel at Re = 24,900.

(3) The contours of isothermal distributions at $x/D_h = 10$ are more strongly concentrated to the position lower than those at $x/D_h = 23$ in the channel with 45° inclined ribs only on the bottom wall. It is supposed that the homogeneous flow at entrance is produced a turbulent flow at a restricted region by the secondary flow formed in the neighbourhood of the ribs at $x/D_h = 10$, however, the turbulent flow is diffused to the whole region inside the channel at $x/D_h = 23$.

Acknowledgements

This work was supported by New University for Regional Innovation Projects.

References

1. J.C. Han, 1988, "Heat Transfer and Friction C haracteristics in Rectangular Channels with Rib Turbulators," Journal of Heat Transfer Vol. 110, pp. 321-328.
2. T. M. Liou, J. J. Hwang, S. H. Chen, 1993, "Simulation and Measurement of Enhanced Turbulent Heat Transfer in a Channel with Periodic Ribs on One Principal Wall," Int. J. Heat Mass and Transfer Vol. 36, No. 2, pp. 507-517.
3. J. C. Han, J. S. Park, 1988, "Developing Heat Transfer in Rectangular Channels with Rib Turbulators," International Journal of Heat and Mass Transfer, Vol. 31, pp. 183-195.
4. M. E. Taslim, T. Li, D. M. Kercher, 1996, "Experimental Heat Transfer and Friction in Channels Roughened with Angled V-Shaped and Discrete Ribs on Two Opposite Walls," ASME J. Turbomachinery, Vol. 118, pp. 20-28.
5. R. Kiml, S. Mochizuki, A. Murata, 2001, "Effects of Rib Arrangements on Heat Transfer and Flow Behavior in a Rectangular Rib-Roughened Passage," ASME J. Heat Transfer, Vol. 123, pp. 675-681.
6. R. L. Webb, E. R. G. Eckert, R. J. Goldstein, 1971, "Heat Transfer and Friction in Tubes with Repeated Rib Roughness," Int. J. Heat and Mass Transfer, Vol. 14, pp. 601-617.
7. W. P. Jones and B. E. Launder, 1972 "The Prediction of Laminarization with a Two-Equation Model of Turbulence, "International

Journal of Heat and Mass Transfer, Vol. 15, pp. 301-314.

8. W. P. Jones and B. E. Launder, 1973, "The Calculation of Low-Reynolds-Number Phenomena with a Two-Equation Model of Turbulence," International Journal of Heat and Mass Transfer, Vol. 16, pp. 1119-1130.
9. H. Schlichting, 1979, "Boundary-Layer Theory," 7th Edition, McGraw-Hill, Inc., New York.
10. V.C. Patel, R., Wolfgang and G. Scheuerer, 1985, "Turbulence Models for Near-Wall and Low Reynolds Number Flows: A Review," AIAA Journal, Vol. 23, pp. 1308-1319.
11. D. Wilcox, 1993, "Turbulence Modeling for CFD," DCW Industries, Inc., La Canada, CA.
12. W.M. Kays, M.E. Crawford, 1980, "Convective Heat and Mass Transfer," 2nd ed., MaGraw-Hill, New York.
13. E. N. Sieder, C. E. Tate, 1936 "Heat Transfer and Pressure Drop of Liquids in Tubes," Ind. Eng. Chem. Vol. 28, pp. 1429.
14. Z. J. Hu, J. Shen, 1996, "Heat transfer Enhancement in a Converging Passage with Discrete Ribs," International Journal of Heat and Mass Transfer, Vol. 39, pp. 1719-1727.